# *Inhibitor-based modulation of huntingtin aggregation reduces fibril toxicity*

Greeshma Jain[*1], Marina Trombetta-Lima[*2,3], Irina Matlahov[1], Hennrique Taborda Ribas[2,4], Amalia M. Dolga[2], Patrick C.A. van der Wel[1,+]

[1] Zernike Institute for Advanced Materials, University of Groningen, Groningen, The Netherlands

[2] Department of Molecular Pharmacology, Faculty of Science and Engineering, Groningen Research Institute of Pharmacy (GRIP), University of Groningen, Groningen, the Netherlands

[3] Department of Biomedical Sciences of Cells and Systems, Section Molecular Cell Biology, University of Groningen, University Medical Center Groningen, Groningen, Netherlands

[4]Graduate Program in Biochemistry Sciences, Department of Biochemistry and Molecular Biology, Federal University of Paraná, Curitiba, PR, Brazil.

* G.J. and M.T-L contributed equally to this work

+ To whom correspondence may be addressed. Email: p.c.a.van.der.wel@rug.nl

**Author Contributions:** G.J., M.T.-L., I.M., H.T.R. performed research; G.J., I.M. performed and analyzed ssNMR and participated in paper editing; G.J., M.T.-L., I.M. analyzed data; A.M.D., P.v.d.W., designed and supervised the research; G.J., M.T-L., A.M.D, P.v.d.W wrote the paper.

## Abstract

Huntington's disease (HD) is a neurodegenerative disorder caused by the expansion of the polyglutamine (polyQ) segment in the exon 1 of the huntingtin (HttEx1) protein. This polyQ expansion leads to protein misfolding and the formation of β-sheet-rich fibrillar aggregates. Several studies have shown that these protein deposits can cause cytotoxicity, suggesting the development of small molecule aggregation inhibitors as potential modulators of HD pathogenesis. This requires a molecular understanding of the impacts of such modulators on the interplay of aggregation, polymorphism and toxic gain-of-function. Here, we study how a polyphenol modulates the HttEx1 aggregation mechanism at sub-stoichiometric ratios. Moreover, we examine how the disrupted aggregation process impacts the protein's misfolded structure and neurotoxic properties. We combine measurements of aggregation kinetics, electron microscopy, solid-state NMR, cytometry, and cytotoxicity assays. A notable delay of protein aggregation was observed even at sub-stoichiometric ratios of curcumin relative to the HttEx1 protein. Mechanistically, extension of the lag phase indicates an impact on the primary nucleation process that underpins the complex HttEx1 aggregation pathway, with an apparent role for β-hairpin formation. Remarkably, the deposits formed (more slowly) in presence of inhibitor displayed reduced toxicity in cultured neuronal cells, seemingly derived from their modulated structures. Thus, curcumin has a multifaceted effect based on delaying the fibril formation, while also changing the toxic properties of formed fibrils. Our findings highlight the ability of small molecule inhibitors to modulate the protein misfolding landscape, with potential implications for treatment strategies in HD and other protein deposition disorders.

***Keywords:*** *Neurodegeneration, amyloid, aggregation inhibitors, Huntington disease*

## Significance Statement

Huntington's disease is an incurable inherited neurodegenerative disorder in which the mutated protein undergoes misfolding and forms fibrillar aggregates. The inhibition of these pathogenic processes represents a major challenge, which also requires an understanding of the complex aggregation mechanism. We observe how small molecule inhibitors can delay formation of toxic deposits by perturbing the aggregation kinetics. Crucially, we find that the modulated aggregation process yields less-toxic fibrils with a different molecular structure. This highlights how inhibition of aggregation process can have unexpected and unintended consequences by yielding novel fibril polymorphs with different biological properties. Analogous multifaceted effects should be considered in the design and testing of aggregation modulators, as they offer both risks and unexpected opportunities as new treatment modalities.

## Introduction

Proper protein folding is vital for living organisms, with small errors in this process resulting in misfolded protein structures that can lead to lethal outcomes in a variety of human diseases (1). In the central nervous system, pathogenic protein deposition is associated with a range of neurodegenerative disorders (2). One such neurodegenerative disease is Huntington's disease (HD) which is one of a whole family of diseases caused by the expansion of the polyglutamine (polyQ) stretch in a specific protein (3). In HD, the polyQ stretch is located near the N-terminus of the mutant huntingtin protein, within the first exon (HttEx1) (Fig 1a). Disease risk is predicted by the extent of polyQ expansion beyond a disease-specific threshold, with the polyQ length inversely correlating with age-of-onset. N-terminal fragments of Htt with an expanded polyQ segment are found in deposits in patients. In prior structural studies it has been found that the aggregates formed by mutant HttEx1 are fibrillar in nature, with a dense and rigid β-sheet core structure formed by the expanded polyQ segment. The basic architecture of this polyQ core displays all the hallmarks of other amyloid-like protein aggregates, such as those formed in other neurodegenerative diseases (4). The Htt-derived protein inclusions are implicated in a variety of toxic mechanisms (5, 6). Yet, there is also convincing evidence that aggregated Htt fragments can form aggregates of different types and sizes, which differ in their toxicity, potentially even in very dramatic ways (7, 8). Given the association of protein aggregation with HD progression, for which it is widely seen as a hallmark biomarker, there is considerable interest in understanding and modulating protein aggregation toward both diagnosis and treatment. This effort benefits from recent breakthroughs in the use of structural techniques to probe the fibrillar species. Recently, we proposed a structural model for the mutant HttEx1 fibril (Fig 1b), in which the polyQ forms a β-sheet rigid core, with N- and C-terminal 'flanking' domains exposed on the fibril surface (9, 10). This model is supported by diverse techniques, including solid-state NMR (ssNMR) and cryo-EM (11–17). The fibril structure has several notable features of relevance to the current study, given expected implications for the fibrils' biological properties. First, the polyQ segment itself forms a rigid dehydrated core structure, within which the Q44 HttEx1 variant was found to feature a β-hairpin fold (14). This translated into a 6-nm fibril core width as observed via negative-stain transmission EM (TEM). Outside this impenetrable core, the fibril is decorated by non-β-sheet 'flanking' segments outside the polyQ itself. These are known as the N-terminal N17 or $Htt^{NT}$ segment, and the C-terminal proline-rich domain (PRD; **Figure 1a**).

A variety of intervention strategies can be envisioned to slow the progression of diseases like Alzheimer's, Parkinson's, and HD: e.g. antibody-based therapeutics, protein-lowering strategies, and small molecule aggregation modulators (18–21). Much recent effort has gone into the protein-lowering approaches, but we hypothesize that methods that target the downstream aggregation process may be a valuable complement, also given recent challenges in clinical tests of Htt lowering in patients. Many small molecules have been studied as modulators of Aβ, α-synuclein, and HttEx1 aggregation (22–24). A common approach is based on naturally occurring polyphenols (25), which are known for their anti-oxidative and anti-inflammatory properties and show therapeutic potential in neurodegenerative disorders (26, 27). Curcumin (Fig. 1c) belongs to the curcuminoid family and is derived from the *Curcuma longa* plant (28). It has been used medicinally for many years because of its antioxidant, anticancer, anti-inflammatory, and neuroprotective

activity (29–31). It has two hydrophobic phenyl rings connected by a flexible linker thus increasing the hydrophobic contacts with multiple target proteins (32, 33). It has yielded promising results in studies on Alzheimer's disease and α-synuclein aggregation (25, 28, 34–36).

In this work we study the modulation of HttEx1 aggregation by curcumin and probe different aspects of how it can modulate amyloid toxicity. In recent years there has been a growing interest in the mechanistic underpinnings of how inhibitors can act on different stages of the aggregation process. This interest derives from the observation that different misfolded species along the aggregation pathway, as well as distinct fibril polymorphs, can have widely varying toxic properties (37, 38). Thus, we were interested in the details of how an aggregation modulating compound changes the aggregation process and fibril polymorphism. We observed that curcumin can delay pathogenic fibril formation, in aggregation studies *in-vitro*. The fibrils formed in the presence of an inhibitor display distinct structural and functional features. By EM and ssNMR measurements, we identify and compare fibril polymorphs formed in presence and absence of inhibitor. Structurally, the differences originate from a different arrangement of the polyQ fibril cores. Crucially, the former species are also found to differ in their neurotoxic effects on cultured neuronal cells, despite being taken up into the cells, indicating the formation of a less-toxic polymorph as a consequence of the inhibitory effects of curcumin.

## Results

### *Curcumin perturbs the aggregation kinetics of HttEx1*

To study the kinetics of HttEx1 aggregation in the presence and absence of curcumin we performed an amyloid-sensitive dye-binding assay using the Thioflavin T (ThT) fluorophore. The ThT dye (**Figure 1d**) is commonly used to detect and quantify β-sheet-rich amyloid fibrils, based on its ability to selectively bind to such fibrils, including polyQ protein aggregates. Monomeric HttEx1 containing a 32-residue polyQ domain (Q32-HttEx1) was obtained by proteolytic cleavage of a soluble fusion protein (9, 13). In absence of curcumin, fibril formation is detected as an increase in ThT fluorescence, with an emission maximum at 490 nm (Fig. 2a), after a lag-phase of 5-6 hours. In presence of curcumin (Fig. 2a) we observe an increased lag-phase, with the increase extending with increasing curcumin concentrations (Fig. 2b). The increased lag phase indicates that curcumin perturbs the primary nucleation process. The curcumin fluorescence curves also show a different steepness in the fibril growth phase. Analogous results were observed also for HttEx1 containing a 44-residue polyQ domain (Fig. S2a). It is important to note that a very precise comparison between the fluorescence curves with and without curcumin is complicated by the fact that curcumin itself shows a dramatic increase in fluorescence as it also binds the fibrils (Fig. S1a, b) (39). The fluorescent properties of ThT and curcumin are difficult to disentangle, but since both show an analogous gain in fluorescence on fibril formation, we used them here interchangeably (see also Fig.S1c in the supporting information).

### *Curcumin results in different morphology of the HttEx1 fibrils*

The aggregation kinetics assay demonstrated that curcumin interacts with the HttEx1 protein at the nucleation phase and causes a delay in the aggregation. Still, after the

extended lag phase, amyloid fibrils appear to form. To verify that the increase in fluorescence intensity indeed stems from amyloid fibrils, and probe for possible differences in their morphology, we employed negative stain TEM. Figure 2 (c, d, e, f) shows TEM micrographs obtained for Q32-HttEx1 aggregated in absence and presence of curcumin. The aggregates formed in absence of curcumin (Fig. 2c) had a fibrillar appearance with a typical width of 10nm (Fig. 2g). In line with prior studies (8–10, 24), the HttEx1 fibrils have a tendency to cluster or bundle together (Fig S3a). Notably, when formed in presence of increasing amounts of curcumin, the fibrils show changes in both width of individual filaments and their propensity to bundle together (Fig. 2d, e, f). Compared to the fibrils formed in absence of curcumin, the fibrils formed in presence of curcumin had a more bundled appearance (Fig. S3b). Fibrils formed in presence of curcumin are relatively narrow (~4nm) (Fig. 3h, I, j), with the observed width distribution dependent on the curcumin concentration, relative to fibrils formed in absence of curcumin (~10nm) (Fig. 2g). Analogous effects were observed when Q44-HttEx1 was aggregated in presence and absence of different concentrations of curcumin (Fig. S2b, c). Thus, the TEM validates that the fluorescence assays detected fibrillar aggregates, whilst revealing a clear curcumin-dependent change in fibril width, morphology, and supramolecular interactions.

### *Curcumin affects the toxicity of HttEx1 fibrils*

Although the debate on the toxic potential of HttEx1 oligomers and fibrils is not settled, contributions from both species to cell death are plausible (40). It has been shown that different fibril polymorphs can have different levels of toxicity (7, 8, 10). This raises the possibility that the fibril polymorphs obtained upon curcumin inhibition differ in toxicity from those that form normally. To examine this question, we challenged mouse hippocampal HT22 and human dopaminergic LUHMES cells with increasing concentrations of pre-formed Q32-HttEx1 fibrils (5 to 25μM). HT22 cells were examined following 24, 48, and 72hrs of Q32-HttEx1 fibril treatment, performing cell viability assessment by MTT assays (Fig. 3a). The normal HttEx1 fibrils display a dose-dependent increase in cytotoxicity in the analyzed periods of treatment. The highest concentration tested (25μM) led to a significant decrease in cell viability after 24h treatment (0.75 ±0.07; p<00.5), while all concentrations tested displayed a significant decrease in cell viability after 48 and 72h treatment. We also tested the effect of the differently structured fibrils formed in the presence of curcumin (at sub stoichiometric molar ratios 0.14 to 0.33 of HttEx1: Curcumin). After 72h of treatment, fibrils formed in the presence of curcumin display a reduced cytotoxic effect in HT22 cells, which is dependent on the curcumin concentration used during the aggregation reaction (Fig. 3b). Noteworthy, treatment with curcumin alone or pre-treatment with curcumin prior to HttEx1 fibril treatment did not significantly alter the observed viability (Fig. S4). We also compared the effects on neuronal network integrity of differentiated human dopaminergic cells, upon treatment with 5μM Q32-HttEx1 fibrils formed in presence and absence of curcumin (at a 0.33 ratio) (Fig. 3c, d). The treatment group that received fibrils formed in absence of curcumin exhibited a substantial decline in the neuronal network integrity compared to the control group. However, the group exposed to fibrils formed upon curcumin inhibition showed a moderate level of damage. Taken together, we observe that the mature HttEx1 fibrils exhibit toxic effects on both neuronal cell types, and that this toxicity is modulated significantly by the curcumin inhibitors, resulting in less toxic fibril species.

It is worth noting that no potentially disruptive techniques or compounds were applied to pro-actively facilitate the fibril uptake into cells, unlike certain prior studies that used e.g. lipofectamine (7). This raises the question of whether the fibrils exerted their toxic effect due to uptake, and whether a reduced toxicity may stem from reduced uptake. To address these questions, we probed the subcellular localization by flow cytometry, based on detection of the His-tag attached to the C-terminal tail of the protein. MAS ssNMR shows this tail to be flexible and exposed on the surface of these HttEx1 fibrils (see Fig. S5-S6) (10, 15, 16). Cells were treated with 5, 15 or 20 μM Q32-HttEx1 fibrils formed in the absence or presence of curcumin (at a 0.33 ratio) for 24h. After treatment, cells were collected and fixed and each condition was divided in two samples, A and B. To distinguish between intracellular and extracellular fibrils bound to the cell membrane, we directly incubated samples A with the anti-His antibody that was restricted to the extracellular environment, while cells in sample B were permeabilized to allow the anti-His antibody to enter the cells (Fig. 3e, f). Our findings indicate that fibrils formed in both the presence and absence of curcumin were detected on the outer surface of cells under non-permeabilized conditions, consistent with previous reports on the presence of Htt fibrils on the cellular surface (41). When the cells are permeabilized we observe an increase in the His-tag signal, which implies that a portion of the fibrils is also found *inside* the neuronal cells. Importantly, this is true for both types of fibrils (formed with and without curcumin inhibition), with no sign of a decreased uptake of the fibrils formed under influence of curcumin.

### *Curcumin changes the structure and dynamics of the fibrils*

Thus, we have observed that curcumin inhibition results in fibrils that change in EM-observed morphology and toxicity. In EM we observed not only changes in clustering behavior of the fibrils, but also a reduction in the width of individual filaments. This indicates a change in the conformation of the fibril core, which defines this characteristic feature of the HttEx1 fibrils (9, 14). To probe for molecular changes in the fibrils, we prepared uniformly $^{13}$C,$^{15}$N-labeled protein fibrils and examined them by ssNMR, using experiments previously used to distinguish fibril polymorphs by differences in structure and dynamics (8, 10). We measured ssNMR spectra of fibrils formed by $^{13}$C,$^{15}$N labeled Q32-HttEx1 in absence and presence of curcumin (protein to curcumin ratio, 1:0.33). 1D $^{13}$C cross-polarization (CP) ssNMR experiments show signals from rigid parts of the fibrils (42). Figure 4a-b shows the $^{13}$CP spectrum for the HttEx1 fibrils grown in absence (green) and presence of curcumin (black). Comparing the two spectra reveals a very high degree of similarity, both in terms of peak positions (chemical shifts) and peak intensities. This observation immediately reveals that the atomic-level architecture within the buried core of the fibrils must be very similar, despite the fibril width differences seen by TEM (Fig S5). This conclusion is reinforced by CP-based 2D ssNMR spectra ($^{13}$C-$^{13}$C DARR (Fig. 4c, d)) showing the polyQ fibril core signals. Thus, while the width of the core changes, the ssNMR peaks match those of untreated fibrils and prior ssNMR studies of other polyQ aggregates (14, 15, 43, 44).

The 1D and 2D spectra contain other peaks not from the polyQ. Most notable are peaks from the proline residues that make up a large part of HttEx1, forming most of the C-terminal PRD. This HttEx1 segment is outside the rigid fibril core, displaying an increased degree of motion that is dependent on the fibril polymorph. Interestingly, the proline peaks for fibrils made in presence of curcumin have a higher CP ssNMR signal intensity,

compared to the Pro signals in curcumin-free conditions (Fig. 4e). This shows that the PRD for the curcumin-modulated fibrils is more rigid than usual. We can also observe this as a change in the relative heights of the polyQ core and PRD signals (Q/P signal ratio; orange arrows in Fig. 4a-b). The change in the Q/P ratio is modest but was reproduced in a separate batch of fibrils, although the precise quantitative change was different (Fig. S6a). The decreased PRD motion could indicate an increase in steric hindrance associated with interactions affecting the PRD segments (more below).

The above data suggest a high similarity in the fibril core structure (at least on the local atomic level; see below), but a more notable effect on the fibril surface dynamics. To probe the latter in more detail we also measured 1D and 2D ssNMR experiments based on the INEPT experiment, which selects for highly flexible residues (Fig. S5, S6, S7). Also here the fibrils prepared in absence and presence of curcumin were highly similar to each other, and closely resembled previously studied HttEx1 fibrils in the literature (9, 10, 14). Peak positions (chemical shifts) appear essentially identical, but variations in peak intensity are observed. These findings point to a difference in dynamics of the (C-terminal) flanking domains, dependent on curcumin inhibition. This observation is reminiscent of prior HttEx1 polymorphism studies by ssNMR, which have revealed that the HttEx1 polymorphs are mostly reflected in changes in the dynamics and interactions among the surface-facing flanking domains (8, 10).

## Discussion

We used curcumin as a small molecule inhibitor and studied its effect on the aggregation kinetics of HttEx1 protein. A clear inhibitory effect was observed that was present even for sub-stoichiometric amounts of curcumin, which is an important feature for a candidate amyloid inhibitor. Mechanistically, the dominant effect was on the aggregation lag phase, which points to curcumin targeting the primary nucleation phase of the aggregation process (45, 46). This is noteworthy as (primary) nucleation is a possible molecular trigger dictating cellular protein aggregation and disease onset in HD (47). Similar effects of curcumin on protein aggregation have been seen with other amyloidogenic polypeptides, with it inhibiting Aβ fibril formation *in-vitro* (34), and inhibiting Aβ oligomerization and aggregation *in vivo* (35). Under the sub-stoichiometric conditions studied here, we see that aggregation is significantly delayed, but that break-through aggregation into fibrils is nonetheless observed. Although not immediately apparent from fluorescence or kinetics analysis, an important finding related to the molecular structure of these break-through fibrils. Both TEM and ssNMR analysis point to changes in the molecular conformation of HttEx1 fibrils, which depend on the curcumin concentration (Fig. 2). We will discuss the nature of the morphological change below, but first address the remarkable impact on the observed cytotoxic properties of the fibrils. We treated HT22 neuronal cells with HttEx1 fibrils formed in presence and absence of curcumin. We observed that both types of fibrils induced progressive reductions in cell viability (Fig. 3b), similar to prior studies showing polyQ and HttEx1 aggregates to be cytotoxic (7, 8, 10). However, the fibrils formed in presence of curcumin induce less cell death compared to the fibrils formed in absence of curcumin. So, the perturbing effect of curcumin on the HttEx1 aggregation process not only delays aggregation, but also leads to the formation of less-toxic fibrils. It is important to note that fibril polymorphism is well-known to be context and condition dependent, such that the extent of this effect may be different under other experimental conditions.

It is worth exploring possible alternative contributions to the observed changes in toxicity. We focus here on the impact of curcumin during the aggregation process *in vitro*, specifically on the resulting fibril structure. This contrasts with studies of the effect of curcumin directly being administered to cells. The data in Fig. 3b are obtained by recovering the fibrils formed in presence of curcumin, washing these fibrils, and adding them to the cultured cells without the further addition of (or treatment with) curcumin. As such we attribute the observed rescue effect primarily to the observed differences in fibril structure. Yet, it is worth noting that our fluorescence assays showed that curcumin not only modulated aggregation but also showed a strong affinity for the formed fibrils (Fig. S1b). As such, the recovered fibrils had curcumin bound to them, raising the possibility of a beneficial effect of the bound curcumin. To understand whether the release of bound curcumin may underpin the observed rescue effect, we also treated cells with different concentration of curcumin in solution. The figure S4 shows that curcumin alone cause no change the cell viability percentage of the cells, thus confirming that the rescue effect is most likely explained by the changed structure of the fibrils.

### *Structural changes in the HttEx1 fibrils*

Our structural studies yielded data on the morphology and structure of the fibrils, pointing to changes as a consequence of the misfolding modulation by curcumin. However, the employed techniques give insights on different microscopic levels: TEM having a resolution at the nm-level or above, whilst ssNMR gives insights on the sub-nm (Å) level. The above-mentioned results may seem to then point in different directions. The TEM showed very clear changes in the fibril diameter, requiring a substantial structural rearrangement of the polyQ segment that forms the fibril core. On the other hand, the ssNMR showed that the polyQ core was unchanged on the atomic level. How can these observations be reconciled?

We will now analyze and discuss the differences in morphology of these Q32-HttEx1 fibrils. The ssNMR data show that the atomic-level structure within the polyQ core is analogous to that in our prior studies. There, we observed that the polyQ core of HttEx1 fibrils contains long extended β-strands, featuring up to 20 Gln residues per strand (9, 17, 43, 48). This corresponds to a β-strand length of 6-7nm (20 Gln), assuming ~3.5Å for each β-strand residue (16). These extended β-strands stand apart from other amyloid fibrils, which often have short β-strand segments, as discussed in more detail in our prior work (9). In Fig. 5a, we see our published model for two polymorphs seen for Q44-HttEx1 fibrils (9), having average widths of ∼6nm (narrow) or ∼15nm (wide). These width values represent TEM width analysis analogous to that performed here. The stain is considered incapable of entering the polyQ β-sheet core, but can penetrate between disordered segments on the fibril surface. As a consequence, we interpret the fibril width seen by TEM (Fig. 2) to reflect the width of the fibril (polyQ) core, without contributions from surface-facing flanking domains.

In analogy, we can propose for the Q32-HttEx1 fibrils formed without curcumin, two models (Fig. 5b) that reflect the expected core width based on the 32-residues-long polyQ segment. To account for the measured 10 nm width with a polyQ cores formed by β-hairpins (as seen for Q44-HttEx1), one would require a multi-filament model given that the hairpin would have a length of ~5 nm. The TEM data could be consistent with this model (i.e., observed width 10-12nm), however the ssNMR data do not show the decrease in proline dynamics due to increased PRD interactions as expected from prior studies (10).

Those studies showed a large restriction of PRD motion when it is involved in multi-filament interactions (8, 10). This should be apparent in the dynamics-sensitive CP- and INEPT-based spectra (42), but was not observed here. Thus, this suggests an alternative tertiary/quaternary structure, not based on the predominance of β-hairpins seen in the Q44-HttEx1 fibrils.

Here it is important to note that various lines of evidence support a model in which β-hairpin-mediated polyQ aggregation is only dominant for long polyQ segments (14, 49, 50). Shorter polyQ segments can and do aggregate, but depend on a nucleation process devoid of β-hairpin formation, expected to result in fibrils featuring monomers forming individual β-strands without turn structures. This is illustrated in Fig. 5b (right), with the N- and C-terminal flanking domains on either side of the core. In the absence of further filament-filament interactions, these flanking domains are solvent exposed and expected to be flexible, as observed by ssNMR (INEPT spectra). This also explains the observed TEM fibril core widths. So, this is the model that best fits the data observed for Q32-HttEx1 aggregated in absence of curcumin. Interestingly, it also lends further support for the idea that a switch to β-hairpin-mediated aggregation may occur close to the HD polyQ expansion threshold length.

In presence of curcumin, we see a clear reduction in the fibril width, reaching widths as low as 4-6nm. This dimension is not compatible with the whole polyQ domain forming a single β-strand, as that would imply a core width of 10-12nm. Thus, we conclude that there must now be a turn in the polyQ domain, yielding a possible β-hairpin structure similar to that seen for Q44-HttEx1. Based on the Q44-HttEx1 data we favor a β-hairpin (i.e., β-turn), but we cannot exclude the possibility of other turn structures (including β-arc) (51). This leads us to the β-hairpin-based model in Fig 5c (right), which perfectly explains our EM data, with β-strands with approximately 14 glutamines for a length of 4.9nm. As noted in prior work (9, 17), the disposition of the flanking segments in such fibril architectures can vary and be harder to predict. We observed a decrease in PRD flanking segment dynamics by ssNMR. This could be explained by increased steric hinderance on the surface of the thinner fibrils, suggesting a dense local clustering of the PRDs.

### *Mechanistic underpinnings of curcumin activity*

We have shown that curcumin perturbs the nucleation phase of the aggregation mechanism, and that this sufficiently changes the Q32-HttEx1 aggregation pathway to yield different fibril polymorphs with reduced toxicity. Here in Fig. 5d, we propose a two-pathway model to illustrate the role of curcumin in altering the aggregation pathway of Q32-HttEx1. The complexity of the HttEx1 aggregation pathway, with its parallel and competing misfolding processes, has been emphasized in prior work (44, 49, 50, 52). Our simplified schematic focuses on the role and fate of the polyQ segment itself. In absence of curcumin, the Q32 polyQ segment favors an aggregation process that does not depend on intramolecular β-hairpin formation, yielding ultimately fibrils with an anti-parallel β-sheet core without β-hairpin. The β-hairpin formation only becomes the dominant pathway if energy gains from intramolecular hydrogen-bond formation are large enough to compensate for entropic losses and the unfavorable formation of a (tight) β-turn. This means that β-hairpins are not favored in short polyQ peptides, but become more likely in longer polyQ (50). Our data suggest that (in absence of curcumin) the dominant (i.e.,

fastest) aggregation process for Q32-HttEx1 involves non-β-hairpin aggregation, resulting in the wide-core fibrils. In contrast, when curcumin is present, this pathway seems be disfavored, leading to thin fibrils featuring short polyQ strands interspersed with turns.

At first glance the favoring of β-hairpins upon inhibition may seem to contradict the argument that β-hairpin-based aggregation should be the faster process, which has been offered as a rationale for the aggregation-enhancing effect of polyQ (50). However, even if β-hairpin-formation is fast(er) than multimeric nucleation *for long polyQ*, the reverse becomes true in short polyQ when β-hairpin formation is unfavorable. Here, our results suggest that curcumin impacts the misfolding process in such a way that the normally faster aggregation process is disfavored, resulting in the normally-slower β-hairpin-based aggregation to become dominant. An interesting implication of these observations is that the Q32-HttEx1 protein, which is close to the HD threshold, is closely balanced between favoring or disfavoring either pathway.

One aspect that is not clear from our current data is the molecular mechanism behind *how* curcumin modulates the misfolding process. As already noted, a big challenge here is the innate complexity of the natural HttEx1 misfolding process, which is not yet fully understood. On the one hand, it is conceivable that curcumin acts via direct interactions with the polyQ domain, destabilizing certain conformations in the soluble protein. Alternatively, it may primarily interact with polyQ oligomers, modulating their structure or formation. On the other hand, also the HttEx1 flanking domains play key roles in the aggregation process. The N-terminal $Htt^{NT}$ segment is famous for driving oligomer formation and boosting aggregation kinetics, in particular at lower concentrations. Thus, it also seems plausible that the effect of (hydrophobic) curcumin could be (in part) explained by interactions with flanking segments, including the amphipathic $Htt^{NT}$ α-helices. These mechanistic details warrant and require further investigation.

### *Modulation of Toxicity*

Our study further reinforces the findings from prior work that HttEx1 fibrils (made *in vitro*) have pathogenic effects on various types of cultured neuronal cells. At the same time, our results add to growing literature that emphasizes that different types of HttEx1 fibrils display different degrees of toxic effects (7, 8, 10). The thinner fibrils made in presence of curcumin are less toxic, compared to the wider fibrils formed in absence of the inhibitor. As discussed, we attribute this difference primarily to a difference in fibril structure rather than the curcumin itself (Fig. S4). It is worth noting that *a priori* we may have expected thinner fibrils to be more fragile and therefore more prone to cellular uptake and toxicity. Yet, our data may support the former (see cytometry data; Fig. 3e), but not the latter. An alternative model is that the pathogenic properties of fibrils may be dictated (in part?) by their surface properties (53, 54), which in turn define their 'interactome' in the cell. It is important to note that the fibrillar interactome does not only include (essential) proteins, but also other cellular components including membranes and lipids.

Here, the ssNMR data are of particular value, as they provide a direct perspective on the fibril surface (10, 12, 55). Dynamic flanking segments decorate the fibril surface and are implicated in protein-protein interactions and protein-lipid interactions (56, 57). Therefore, a restructuring of the fibrils, which is seen to change the PRD dynamics, can change these cellular interactions. We propose that this may play a role in contributing to the reduced toxicity of the curcumin-modulated HttEx1 fibrils.

The targeting of the protein aggregation process itself is a potential strategy for treating HD, with several drugs in clinical trial for slowing HD progression (58). Small molecules that delay or inhibit protein aggregation could be a valuable strategy (4, 18, 24). The current study shows that certain compounds might have a multifaceted beneficial effect, by not only delaying aggregation but also making any break-through aggregates less toxic. An important caveat of this finding is that one may also observe the opposite phenomenon, depending on the exact mechanism of inhibitory action and (cellular) context. It seems plausible that under certain conditions new polymorphs could be formed that display increased rather than decreased toxic activity. This is similarly possible when translating *in vitro* studies (as done here) to the aggregation of HttEx1 in cells or *in vivo*. These considerations should be kept in mind in such studies and warrant further investigation.

## Materials and Methods

**Protein production and aggregation**: The maltose-binding domain (MBP)-fusion protein MBP-Q32-HttEx1, featuring wild-type HttEx1 with 32 consecutive glutamine residues within the polyQ domain was sub-cloned into a pMALc5x plasmid by Genscript (Piscataway, NJ), as previously described (9). The purified fused protein was cleaved by treating it with Factor Xa (FXa; Promega, Madison, WI) at room temperature. After aggregation of the released monomers for 4 days, resulting protein aggregates were pelleted by centrifugation at 3,000xg for 20 min. The protocol is described in detail in the SI Materials and Methods.

**Solid-state NMR**: For MAS ssNMR, uniformly $^{13}$C- and $^{15}$N-labelled (U-$^{13}$C,$^{15}$N) purified fusion protein was cleaved and allowed to aggregate over 4 days, after which the fibrils were pelleted down at 3,000xg for 20 min and resuspended in 1ml PBS (pH 7.4) containing 0.01% (w/w) sodium azide. The buffer was sterilized by filtration through 0.22μm filters (MF-Millipore, Ireland). MAS ssNMR samples were packed in 3.2 mm MAS sample holders (Bruker Biospin, Billerica, MA, and CortecNet, Brooklyn, NY) using a home-built ultracentrifugal sample packing tool operated for 1 h at 150,000xg (59). The supernatant was discarded, and pelleted fibrils were washed at least three times with PBS buffer prior to sealing the MAS rotor. Samples were studied by MAS ssNMR in a hydrated and unfrozen state. All the experiments with Batch 1and Batch 2 fibril samples were acquired on Bruker Avance 600 MHz spectrometer, equipped with a 3.2 mm MAS probe with an HCN Efree coil (Bruker Biopsin). More experimental details are in the SI Table 1.

**ThT Assay:** For aggregation kinetics analysis, 61uM MBP-Q32-HttEx1 protein was used, with cleavage performed with FXa at a 400:1 molar ratio (HttEx1: FXa). ThT was included in the black polystyrene, clear bottom, 96-well plates (Corning, U.S.A) at a final concentration of 15μM. Curcumin was added to a final concentration of 8.5uM, 12uM, and 20uM. Samples were mixed gently and then measured on a TECAN Spark 10M microplate reader. Excitation occurred at 442 nm and emission was recorded from 482-492nm, with excitation and emission bandwidths of 10nm. More details are in the SI Materials and Methods.

**Transmission Electron Microscopy:** Transmission electron microscopy (TEM) was performed on Q32-HttEx1 and Q44-HttEx1 protein that was allowed to aggregate at room temperature for 96 hours, in the absence and presence of different concentrations of curcumin. The fibril samples were deposited on plain carbon support film on 200 mesh copper grids (SKU FCF200-Cu-50, Electron Microscopy Sciences, Hatfield, PA) after glow-discharge for 0.5 -1 min. The negative staining agent used was 2% (w/v) uranyl acetate. The excess stain was removed by blotting and the grid air dried. The images were recorded on a Philips CM120 electron microscope operating at 120kV. The fibril widths were measured transverse to the fiber long axis using the straight Free-hand tool of Fiji (60). More details are in the SI Materials and Methods.

**Cell Culture:** Mouse HT-22 hippocampal cell lines and Lund human mesencephalic cells (LUHMES)- differentiated neuronal cells were kindly provided by Prof. Culmsee, University of Marburg, Germany. HT22 cells were cultured in Dulbecco's Modified Eagle Medium (Gibco, ThermoFisher Scientific, Landsmeer, The Netherlands) supplemented with 1% pyruvate (ThermoFisher Scientific), 10% fetal bovine serum (GE Healthcare Life Sciences, Eindhoven, the Netherlands), and 100U/mL penicillin-streptomycin. LUHMES cells were cultured in Advanced DMEM/F12 (Gibco), supplemented with 200 mM L-Glutamine (Gibco), 1x N2 Supplement (Gibco), 100 µg/ml FGF (PeproTech, Cranbury, USA), and 1x penicillin/streptomycin solution (Gibco). LUHMES cells were differentiated to dopaminergic neurons before the treatments as described before (61, 62). Cells were maintained at 37° and 5% $CO_2$. Cells were used for experiments for at most 10 passages after thawing and regularly checked for Mycoplasma infection.

**Cell viability assay:** Cell viability was assessed using MTT (3-(4,5-dimethyl-2-thiazolyl)-2,5-diphenyl-2H-tetrazolium bromide; Sigma-Aldrich) reduction assay (63). HT22 cells were seeded in p96 wells at a density of $9.10^3$ cells/well. After 24h of seeding, the cells were treated with 0, 5, 15 or 25 µM of pre-formed Q32-HttEx1 fibrils diluted in culture medium and incubated for 24, 48 or 72h. For endpoint analysis, cells were incubated with 0.5 mg/ mL MTT for 1 h at 37°C and 5% $CO_2$. The supernatant was removed and the plate was stored at -20°C for at least two hours. Afterwards, 100µL of dimethyl sulfoxide (DMSO; Sigma-Aldrich) was added to each well and the plate was incubated for 1 h under mild shaking at 37 °C. The absorbance of each well was determined at 570 nm with reference background absorbance at 630 nm using a Synergy H1 Multi-Mode reader (Biotek, Winooski, US). Absorption values were normalized to the average of the untreated control to determine cell viability in reference to the untreated control (reference value 1).

**Neuronal network integrity assay:** LUHMES cells were seeded in pre-coated 48-well Nuclon TM plates at a density of $5.10^4$ cells/well. After 6 days of differentiation, the cells were treated with 5µM of pre-formed HttEx1 fibrils, and incubated curcumin. The cells were treated for 24 hours at 37°C and 5% $CO_2$. Neuronal network integrity was determined as previously described (64). Briefly, cells were stained with 1 µM Calcein-AM (Sigma-Aldrich) and 1µg/mL Hoestch (Invitrogen, ThermoFisher) for live cell imaging. The neuronal network was imaged with the Zeiss Cell Discoverer 7 (Zeiss, Oberkochen, Germany) and analyzed with the Fiji Macro Plug-In NeurphologyJ Interactive, with neurite area as the dependent variable (65).

**Flow cytometry:** To estimate the subcellular localization of the Q32-HttEx1 fibrils, the presence of the C-terminal His-tag of fibrillar Q32-HttEx1 was detected by flow cytometry. HT22 cells were treated with 5, 15 or 20 μM Q32-HttEx1 formed in the absence or presence of curcumin (at a 0.33 ratio) for 24h. Cells were harvested with trypsin and permeabilized or not with 0.1% Triton-X (Sigma) in PBS for 15 min at RT. Next, cells were blocked with 1% BSA (Sigma) in PBS for 1h, followed by incubation with 1μg/mL. The His-Tag antibody (Cat# A00186S, GenScript, New Jersey, US) for 2h at RT. Secondary antibody Alexa Fluor 488 nm Donkey anti-mouse (Jackson, Cambridgeshire, UK) was incubated for 2h, RT. Fluorescence was measured at 690/50 nm in the CytoFLEX benchtop flow cytometer (Beckman Coulter Life Sciences, Indianapolis, US). Analysis was performed using FlowJo v9.0 (Becton, Dickinson and Company, Franklin Lakes, US).

## Acknowledgments

We thank Dr. Marc Stuart for the Electron Microscopy facility. We also thank Dr. Alessia Lasorsa for her help with the solid-state NMR experiments, and Gea Schuurman- Wolters for her help with the wet-lab instruments. We acknowledge funding from The CampagneTeam Huntington and CHDI Foundation (contract A-17778).

## References

1. C. B. Anfinsen, Principles that govern the folding of protein chains. *Science* **181**, 223–230 (1973).

2. C. A. Ross, M. A. Poirier, Protein aggregation and neurodegenerative disease. *Nat. Med.* **10**, S10–S17 (2004).

3. D. M. Hatters, Protein misfolding inside cells: The case of huntingtin and Huntington's disease. *IUBMB Life* **60**, 724–728 (2008).

4. E. Scherzinger, *et al.*, Self-assembly of polyglutamine-containing huntingtin fragments into amyloid-like fibrils: implications for Huntington's disease pathology. *Proc. Natl. Acad. Sci. U. S. A.* **96**, 4604–4609 (1999).

5. F. C. Nucifora, *et al.*, Interference by huntingtin and atrophin-1 with cbp-mediated transcription leading to cellular toxicity. *Science* **291**, 2423–2428 (2001).

6. J. S. Steffan, *et al.*, The Huntington's disease protein interacts with p53 and CREB-binding protein and represses transcription. *Proc. Natl. Acad. Sci. U. S. A.* **97**, 6763–6768 (2000).

7. Y. Nekooki-Machida, *et al.*, Distinct conformations of in vitro and in vivo amyloids of huntingtin-exon1 show different cytotoxicity. *Proc. Natl. Acad. Sci.* **106**, 9679–9684 (2009).

8. J. Mario Isas, *et al.*, Huntingtin fibrils with different toxicity, structure, and seeding potential can be interconverted. *Nat. Commun.* **12**, 4272 (2021).

9. J. C. Boatz, *et al.*, Protofilament Structure and Supramolecular Polymorphism of Aggregated Mutant Huntingtin Exon 1. *J. Mol. Biol.* **432**, 4722–4744 (2020).

10. H.-K. Lin, *et al.*, Fibril polymorphism affects immobilized non-amyloid flanking domains of huntingtin exon1 rather than its polyglutamine core. *Nat. Commun.* **8**, 15462 (2017).

11. C. W. Bugg, J. M. Isas, T. Fischer, P. H. Patterson, R. Langen, Structural Features and Domain Organization of Huntingtin Fibrils *. *J. Biol. Chem.* **287**, 31739–31746 (2012).

12. A. S. Falk, *et al.*, Structural Model of the Proline-Rich Domain of Huntingtin Exon-1 Fibrils. *Biophys. J.* **119**, 2019–2028 (2020).

13. C. L. Hoop, *et al.*, Polyglutamine Amyloid Core Boundaries and Flanking Domain Dynamics in Huntingtin Fragment Fibrils Determined by Solid-State Nuclear Magnetic Resonance. *Biochemistry* **53**, 6653–6666 (2014).

14. C. L. Hoop, *et al.*, Huntingtin exon 1 fibrils feature an interdigitated β-hairpin–based polyglutamine core. *Proc. Natl. Acad. Sci.* **113**, 1546–1551 (2016).

15. J. M. Isas, R. Langen, A. B. Siemer, Solid-State Nuclear Magnetic Resonance on the Static and Dynamic Domains of Huntingtin Exon-1 Fibrils. *Biochemistry* **54**, 3942–3949 (2015).

16. J. M. Isas, A. Langen, M. C. Isas, N. K. Pandey, A. B. Siemer, Formation and Structure of Wild Type Huntingtin Exon-1 Fibrils. *Biochemistry* **56**, 3579–3586 (2017).

17. S. Nazarov, A. Chiki, D. Boudeffa, H. A. Lashuel, Structural Basis of Huntingtin Fibril Polymorphism Revealed by Cryogenic Electron Microscopy of Exon 1 HTT Fibrils. *J. Am. Chem. Soc.* **144**, 10723–10735 (2022).

18. V. Heiser, *et al.*, Inhibition of huntingtin fibrillogenesis by specific antibodies and small molecules: implications for Huntington's disease therapy. *Proc. Natl. Acad. Sci. U. S. A.* **97**, 6739–6744 (2000).

19. S. Mafimoghaddam, *et al.*, Suppression of amyloid-β fibril growth by drug-engineered polymorph transformation. *J. Biol. Chem.* **298**, 102662 (2022).

20. Y. J. Yu, R. J. Watts, Developing therapeutic antibodies for neurodegenerative disease. *Neurotherapeutics.* **10**, 459–472 (2013).

21. X. Zhang, *et al.*, A potent small molecule inhibits polyglutamine aggregation in Huntington's disease neurons and suppresses neurodegeneration in vivo. *Proc. Natl. Acad. Sci. U. S. A.* **102**, 892–897 (2005).

22. D. E. Ehrnhoefer, *et al.*, EGCG redirects amyloidogenic polypeptides into unstructured, off-pathway oligomers. *Nat. Struct. Mol. Biol.* **15**, 558–566 (2008).

23. J. Pujols, *et al.*, Small molecule inhibits α-synuclein aggregation, disrupts amyloid fibrils, and prevents degeneration of dopaminergic neurons. *Proc. Natl. Acad. Sci. U. S. A.* **115**, 10481–10486 (2018).

24. A. S. Wagner, *et al.*, Self-assembly of Mutant Huntingtin Exon-1 Fragments into Large Complex Fibrillar Structures Involves Nucleated Branching. *J. Mol. Biol.* **430**, 1725–1744 (2018).

25. A. Thapa, S. D. Jett, E. Y. Chi, Curcumin Attenuates Amyloid-β Aggregate Toxicity and Modulates Amyloid-β Aggregation Pathway. *ACS Chem. Neurosci.* **7**, 56–68 (2016).

26. A. Ebrahimi, H. Schluesener, Natural polyphenols against neurodegenerative disorders: Potentials and pitfalls. *Ageing Res. Rev.* **11**, 329–345 (2012).

27. C. Ramassamy, Emerging role of polyphenolic compounds in the treatment of neurodegenerative diseases: a review of their intracellular targets. *Eur. J. Pharmacol.* **545**, 51–64 (2006).

28. N. Pandey, J. Strider, W. C. Nolan, S. X. Yan, J. E. Galvin, Curcumin inhibits aggregation of alpha-synuclein. *Acta Neuropathol. (Berl.)* **115**, 479–489 (2008).

29. M. C. Fadus, C. Lau, J. Bikhchandani, H. T. Lynch, Curcumin: An age-old anti-inflammatory and anti-neoplastic agent. *J. Tradit. Complement. Med.* **7**, 339–346 (2017).

30. H. Kim, *et al.*, Effects of Naturally Occurring Compounds on Fibril Formation and Oxidative Stress of β-Amyloid. *J. Agric. Food Chem.* **53**, 8537–8541 (2005).

31. K. M. Nelson, *et al.*, The Essential Medicinal Chemistry of Curcumin. *J. Med. Chem.* **60**, 1620–1637 (2017).

32. S. C. Gupta, *et al.*, Multitargeting by curcumin as revealed by molecular interaction studies. *Nat. Prod. Rep.* **28**, 1937–1955 (2011).

33. M. Hatamipour, T. P. Johnston, A. Sahebkar, One Molecule, Many Targets and Numerous Effects: The Pleiotropy of Curcumin Lies in its Chemical Structure. *Curr. Pharm. Des.* **24**, 2129–2136 (2018).

34. K. Ono, K. Hasegawa, H. Naiki, M. Yamada, Curcumin has potent anti-amyloidogenic effects for Alzheimer's β-amyloid fibrils in vitro. *J. Neurosci. Res.* **75**, 742–750 (2004).

35. F. Yang, *et al.*, Curcumin Inhibits Formation of Amyloid β Oligomers and Fibrils, Binds Plaques, and Reduces Amyloid in Vivo*. *J. Biol. Chem.* **280**, 5892–5901 (2005).

36. P. K. Singh, *et al.*, Curcumin modulates α-synuclein aggregation and toxicity. *ACS Chem. Neurosci.* **4**, 393–407 (2013).

37. Y. S. Eisele, *et al.*, Targeting protein aggregation for the treatment of degenerative diseases. *Nat. Rev. Drug Discov.* **14**, 759–780 (2015).

38. M. G. Iadanza, M. P. Jackson, E. W. Hewitt, N. A. Ranson, S. E. Radford, A new era for understanding amyloid structures and disease. *Nat. Rev. Mol. Cell Biol.* **19**, 755–773 (2018).

39. S. A. Hudson, H. Ecroyd, T. W. Kee, J. A. Carver, The thioflavin T fluorescence assay for amyloid fibril detection can be biased by the presence of exogenous compounds. *FEBS J.* **276**, 5960–5972 (2009).

40. S. Kim, K.-T. Kim, Therapeutic Approaches for Inhibition of Protein Aggregation in Huntington's Disease. *Exp. Neurobiol.* **23**, 36–44 (2014).

41. E. Monsellier, L. Bousset, R. Melki, α-Synuclein and huntingtin exon 1 amyloid fibrils bind laterally to the cellular membrane. *Sci. Rep.* **6**, 19180 (2016).

42. I. Matlahov, P. C. A. van der Wel, Hidden motions and motion-induced invisibility: Dynamics-based spectral editing in solid-state NMR. *Methods San Diego Calif* **148**, 123–135 (2018).

43. R. Schneider, *et al.*, Structural characterization of polyglutamine fibrils by solid-state NMR spectroscopy. *J. Mol. Biol.* **412**, 121–136 (2011).

44. V. N. Sivanandam, *et al.*, The aggregation-enhancing huntingtin N-terminus is helical in amyloid fibrils. *J Am Chem Soc* **133**, 4558–4566 (2011).

45. P. Arosio, T. P. J. Knowles, S. Linse, On the lag phase in amyloid fibril formation. *Phys. Chem. Chem. Phys.* **17**, 7606–7618 (2015).

46. T. C. T. Michaels, *et al.*, Chemical Kinetics for Bridging Molecular Mechanisms and Macroscopic Measurements of Amyloid Fibril Formation. *Annu. Rev. Phys. Chem.* **69**, 273–298 (2018).

47. T. Sinnige, *et al.*, Kinetic analysis reveals that independent nucleation events determine the progression of polyglutamine aggregation in C. elegans. *Proc. Natl. Acad. Sci.* **118**, e2021888118 (2021).

48. D. Sharma, L. M. Shinchuk, H. Inouye, R. Wetzel, D. A. Kirschner, Polyglutamine homopolymers having 8-45 residues form slablike beta-crystallite assemblies. *Proteins* **61**, 398–411 (2005).

49. I. Matlahov, P. C. van der Wel, Conformational studies of pathogenic expanded polyglutamine protein deposits from Huntington's disease. *Exp Biol Med Maywood* **244**, 1584–1595 (2019).

50. K. Kar, *et al.*, β-hairpin-mediated nucleation of polyglutamine amyloid formation. *J Mol Biol* **425**, 1183–1197 (2013).

51. A. V. Kajava, U. Baxa, A. C. Steven, Beta arcades: recurring motifs in naturally occurring and disease-related amyloid fibrils. *FASEB J. Off. Publ. Fed. Am. Soc. Exp. Biol.* **24**, 1311–1319 (2010).

52. M. Jayaraman, *et al.*, Kinetically competing huntingtin aggregation pathways control amyloid polymorphism and properties. *Biochemistry* **51**, 2706–2716 (2012).

53. R. S. Trevino, *et al.*, Fibrillar Structure and Charge Determine the Interaction of Polyglutamine Protein Aggregates with the Cell Surface. *J Biol Chem* **287**, 29722–29728 (2012).

54. Y. Yoshiike, T. Akagi, A. Takashima, Surface structure of amyloid-beta fibrils contributes to cytotoxicity. *Biochemistry* **46**, 9805–9812 (2007).

55. I. Matlahov, J. C. Boatz, P. C.A. van der Wel, Selective observation of semi-rigid non-core residues in dynamically complex mutant huntingtin protein fibrils. *J. Struct. Biol. X* **6**, 100077 (2022).

56. J. Ko, *et al.*, Identification of distinct conformations associated with monomers and fibril assemblies of mutant huntingtin. *Hum. Mol. Genet.* **27**, 2330–2343 (2018).

57. A. E. Posey, *et al.*, Profilin reduces aggregation and phase separation of huntingtin N-terminal fragments by preferentially binding to soluble monomers and oligomers. *J. Biol. Chem.* **293**, 3734–3746 (2018).

58. F. O. Walker, Huntington's disease. *The Lancet* **369**, 218–228 (2007).

59. A. Mandal, J. C. Boatz, T. B. Wheeler, P. C. A. van der Wel, On the use of ultracentrifugal devices for routine sample preparation in biomolecular magic-angle-spinning NMR. *J Biomol NMR* **67**, 165–178 (2017).

60. C. A. Schneider, W. S. Rasband, K. W. Eliceiri, NIH Image to ImageJ: 25 years of image analysis. *Nat. Methods* **9**, 671–675 (2012).

61. A. M. Dolga, *et al.*, Subcellular expression and neuroprotective effects of SK channels in human dopaminergic neurons. *Cell Death Dis.* **5**, e999 (2014).

62. J. Lotharius, *et al.*, Effect of mutant alpha-synuclein on dopamine homeostasis in a new human mesencephalic cell line. *J. Biol. Chem.* **277**, 38884–38894 (2002).

63. M. Richter, *et al.*, Activation of SK2 channels preserves ER $Ca^{2+}$ homeostasis and protects against ER stress-induced cell death. *Cell Death Differ.* **23**, 814–827 (2016).

64. P. Kranaster, *et al.*, Time and space-resolved quantification of plasma membrane sialylation for measurements of cell function and neurotoxicity. *Arch. Toxicol.* **94**, 449–467 (2020).

65. S.-Y. Ho, *et al.*, NeurphologyJ: an automatic neuronal morphology quantification method and its application in pharmacological discovery. *BMC Bioinformatics* **12**, 230 (2011).

## Figures

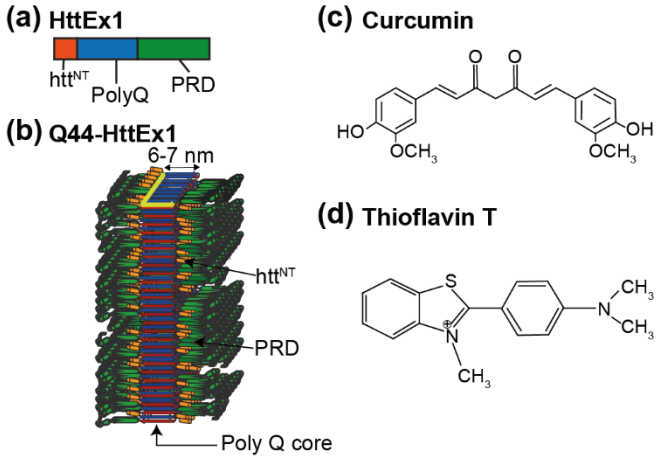


**Figure 1. Structures of Htt exon 1, curcumin and Thioflavin T (ThT).** (a) Domain structure of HttEx1, showing the central polyQ segment (blue) as well as the N-terminal ($htt^{NT}$; orange) and C-terminal flanking segments (proline-rich domain; PRD; green). (b) Model of the previously determined fibril architecture of Q44-HttEx1 forming single-filament fibrils. Indicated domains: $htt^{NT}$ (orange; α-helix), polyQ (red and blue; β-sheet), and PRD (green; PPII helices). (c) Chemical structures of curcumin and (d) Thioflavin T. Panel b was adapted with permission from (9).

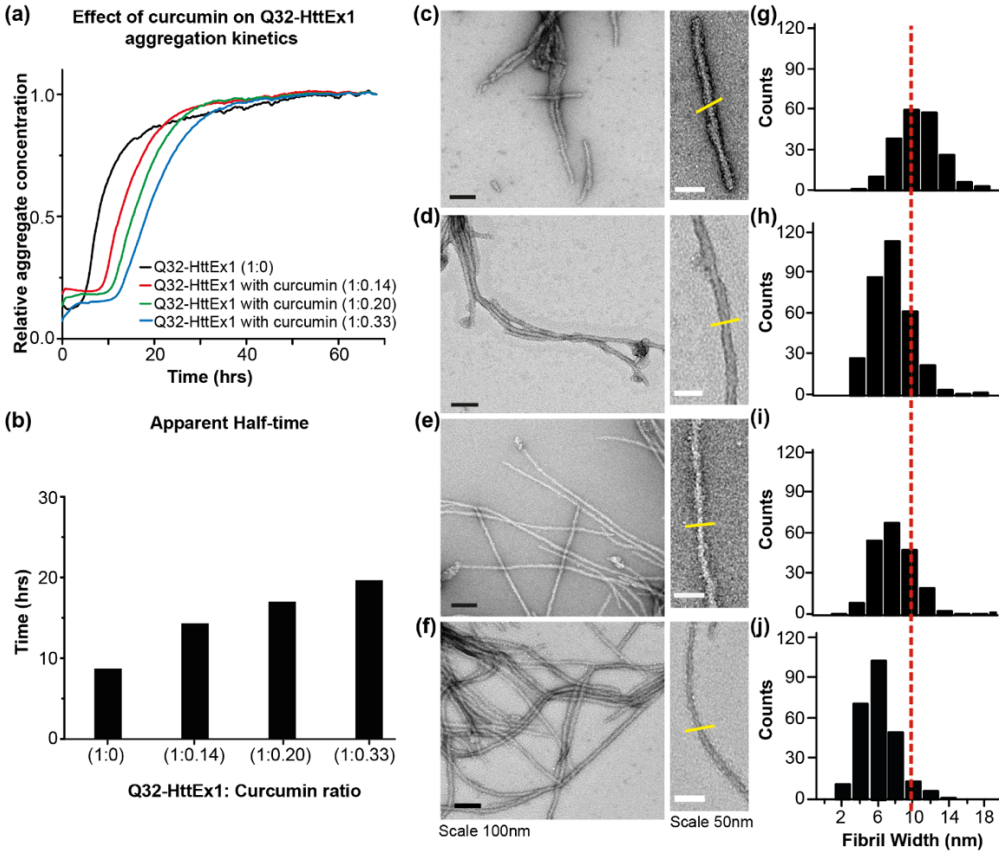


**Figure 2. Fluorescence assays and TEM analysis of HttEx1 aggregation in presence and absence of curcumin.** (a) Q32-HttEx1 (61μM) aggregation was monitored by ThT assays, measuring fluorescence in the presence and absence of curcumin (molar ratio indicated). (b) Apparent half-time as a function of the curcumin concentration. (c-f) TEM micrographs of 61μm Q32-HttEx1 fibrils, formed (c) without curcumin; (d) with 8.5μM curcumin; (e) with 12μM curcumin; (f) with 20μM curcumin. The yellow lines perpendicular to the fibril axis mark locations of fibril width measurements. (g-j) TEM-based fibril core width histograms corresponding to samples in (c-f). The vertical dashed line marks the average width of fibrils formed in absence of curcumin.

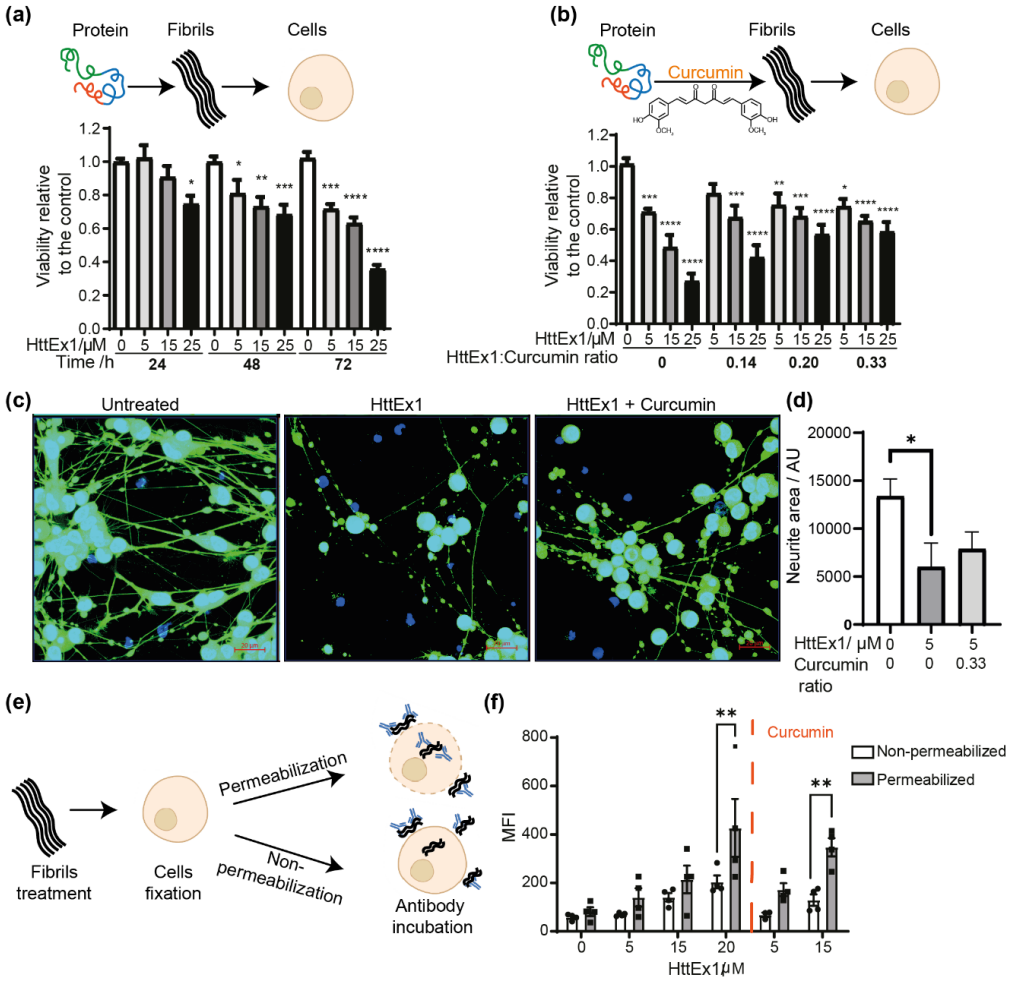


**Figure 3. Cytotoxicity and cellular localization of Q32-HttEx1 fibrils prepared in the presence and absence of curcumin.** (a) Cell viability assay was performed following a 24, 48, and 72h exposure of HT22 cells with varying concentrations of HttEx1 fibrils and HttEx1 fibrils prepared in presence of different ratios of curcumin. (b) Cell viability assay was performed following a 72hrs exposure of HT22 cells with varying concentrations of HttEx1 fibrils and HttEx1 fibrils prepared with different ratios of curcumin (as indicated). (c) Representative pictures of differentiated LUHMES cells exposed for 24h to HttEx1 fibrils formed in absence or presence of curcumin. (d) Total neurite length normalized by nuclei number (e) Schematic representation of the experimental workflow for the determination of HttEx1 fibrils' cellular localization. (f) Detection of HttEx1 His-tag after post-fixing permeabilization of cells treated with HttEx1 prepared in the presence or absence of curcumin. N>3 for each experiment. One-way ANOVA followed by Dunnett's multiple comparisons test. Bars represent the mean ±SD. *stands for p<0.005. ** stands for p<0.01. *** stands for p<0.001. **** stands for p<0.0001.

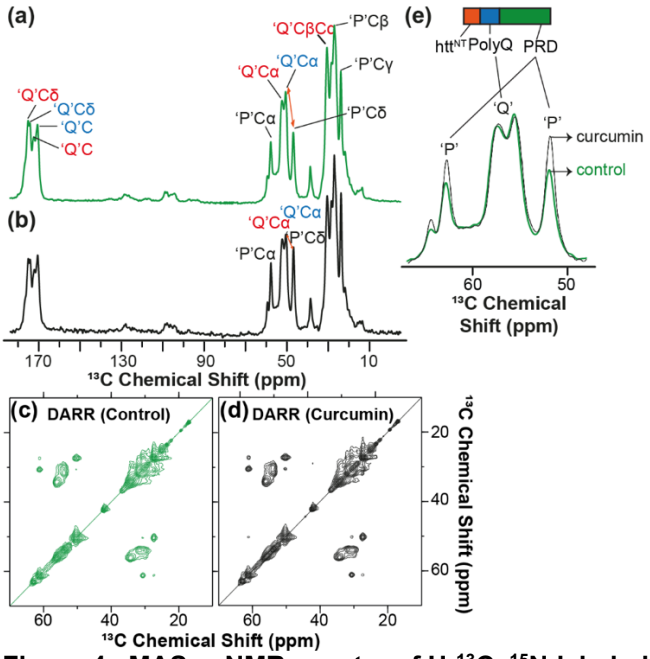


**Figure 4. MAS ssNMR spectra of U-$^{13}$C, $^{15}$N-labeled Q32-HttEx1 fibrils.** (a) 1D $^{13}$C CP spectra of fibrils formed at room temperature without curcumin (green), and (b) with curcumin (at the protein: curcumin ratio of 1:0.33) (black). The spinning frequency was 10 kHz. (d) 2D $^{13}$C -$^{13}$C DARR spectrum for U-$^{13}$C, $^{15}$N Q32-HttEx1 fibrils obtained at 13 kHz MAS and 25ms of DARR mixing. (e) 2D $^{13}$C -$^{13}$C DARR spectrum for U-$^{13}$C, $^{15}$N Q32-HttEx1fibrils prepared in presence of curcumin (1:0.33) obtained at 13 kHz MAS and 25ms of DARR mixing. (e) Zoomed-in overlay of 1D spectral regions showing Gln C$\alpha$ peaks (middle) and Pro peaks, from spectra (a)-(b). The NMR measurements were performed at 275K on a 600MHz spectrometer.

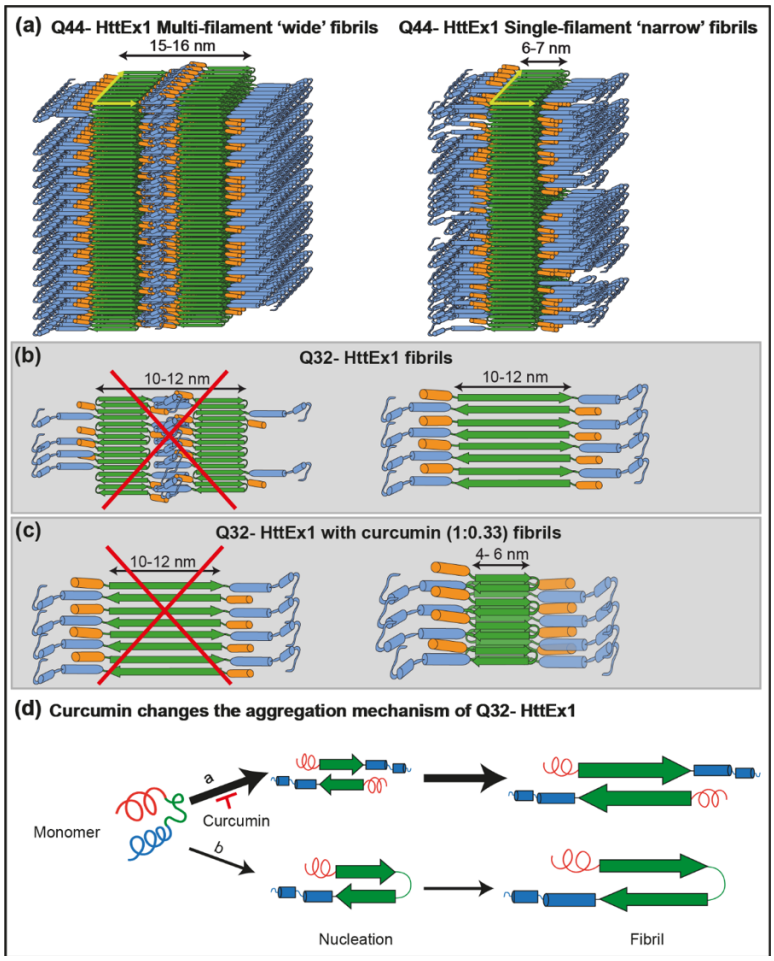


**Figure 5. Models for HttEx1 fibril structure and assembly.** (a) Existing models of Q44-HttEx1 multi-filament 'wide' fibrils (left) and a single-filament 'narrow' fibrils (right) (9). Both models show a β-sheet core formed by polyQ segments in a β-hairpin fold. (b) Hypothetical models of Q32-HttEx1 fibrils formed in absence of curcumin, which match the observed TEM core width: double-filament fibrils with β-hairpins (left) or single-filament fibrils without (right). The ssNMR data show flexible PRD which is not consistent with the former model. (c) Hypothetical models of Q32-HttEx1 fibrils formed in presence of curcumin. Left model assumes an extended β-strand (no β-hairpin), but the predicted core diameter does not match TEM width. The model on the right shows the polyQ segment as a single filament featuring β-hairpins. (d) Schematic of the complex HttEx1 aggregation pathway, with competing mechanisms without (top) and with β-hairpin formation (bottom). The former pathway is dominant in absence of curcumin, but is inhibited by curcumin. Observed 'break-through' fibril formation (upon curcumin inhibition) results in fibril cores with a narrower width, consistent with the presence of β-hairpins. Panel b was adapted with permission from ref. (9).